Numerical Solution of Strong Radiation Gasdynamic Interactions in a Hydrogen-Seedant Mixture

Charles L. Merkle,* Gregory A. Molvik,† and Eric J.-H. Shaw†
Pennsylvania State University, University Park, Pennsylvania

The absorption of laser energy in a flowing gas is analyzed by means of a two-dimensional numerical model. Gas properties for equilibrium hydrogen seeded with a trace amount of cesium are used to provide low-temperature absorption. Radiation loss from the gas is ignored. The incoming 10.6 μm beam has a Gaussian intensity profile and converges to a focus inside the nozzle. The conditions calculated correspond to fairly high subsonic Mach numbers where relatively low temperature rises are encountered. Parametric studies of laser power variations, gas velocity changes, inlet temperature changes, and pressure level changes are presented. In addition, two different focal lengths are used. The results show that increasing the pressure, the laser power, or the inlet temperature causes the absorption region to move forward in the nozzle, while decreasing the gas velocity causes the peak temperature to increase. However, both the peak temperature and the location of the absorption region are dependent upon a complex balance between many competing factors. The results suggest that stable flowfields are produced even when substantial fractions of the heat is absorbed aft of the focal point. In studying the effects of pressure or gas velocity changes, it is noted that the laser power should be normalized by the mass flow. Finally, the hotter temperatures on the centerline cause preferential absorption, so that an initially Gaussian intensity profile can reach zero intensity on the centerline while substantial power remains in the outer portion of the beam.

Introduction

THE interaction between an intense beam of electromagnetic energy and a flowing gas is highly nonlinear. At atmospheric pressure, the absorptivity of a typical gas ranges from as low as 10^{-12}–10^{-15}/m at room temperature to peak values of more than 10^{-2}/m at elevated temperatures. This absorptivity variation of more than 10 orders of magnitude is the primary reason for the strong nonlinearity. The interactions to be considered in the present paper are stimulated by an interest in laser propulsion [1-4] that encompasses this entire range of absorptivities.

In laser propulsion applications, a working fluid is heated by direct absorption of an incoming laser beam and is then exhausted through a converging-diverging nozzle to produce thrust. Pure hydrogen or hydrogen mixed with trace amounts of other gases represent likely choices for the working fluid.[1,5] Current laboratory experiments are being performed with argon[6,7] because of the ease with which absorption can be accomplished in this gas, as well as with hydrogen.[8] Argon and pure hydrogen behave similarly in that the primary absorption mechanism is inverse bremsstrahlung and typical temperatures in these two gases are 15,000 and 18,000 K, respectively. Hydrogen-seedant mixtures are selected to have enhanced absorptivity at lower temperatures so that peak temperatures can be reduced to around 6000 K.[5] Gases such as carbon monoxide and water vapor provide low-temperature absorption through their molecular vibration levels. Trace amounts of cesium can also be effective at low temperatures because of cesium's low ionization potential.

In the laser propulsion concept, the radiation gasdynamic interaction is generally confined to the central part of the flow by focusing the beam in the upstream section of the nozzle as shown in Fig. 1. This configuration not only protects the nozzle walls, but the beam convergence also provides stability to the absorption region.[9] Downstream of the absorption region, mixing between the hot central core and the cool outer gases is desirable to maximize thrust and possibly to minimize recombination losses.

Although the problem illustrated in Fig. 1 and described above is clearly two-dimensional, most previous analyses have been one-dimensional in nature. In fact, most analyses of the absorption process have treated a collimated beam in a constant-area duct.[9-12] In these constant-area analyses, the equations of motion are simplified to a single ordinary differential equation by a low Mach number assumption. This approach rules out the effects of beam convergence and radial temperature gradients, but was necessitated by the complexity of the problem. More recently, the present author has applied an implicit numerical algorithm to the laser flowfield interaction in a one-dimensional nozzle,[13] but, even in the case where heat addition is specified (the absorption uncoupled from the flow), it has been shown[14] that contemporary algorithms[15] fail to converge at the maximum heating rates of interest. Some of these difficulties have since been overcome and the present paper addresses the two-dimensional problem.

Two simplified two-dimensional analyses have also been reported. In Ref. 16, the approximate, low Mach number analysis was extended to allow for a two-dimensional temperature field in the presence of a uniform flowfield ($\rho u = \text{const}$, $v = 0$). The complete fluid dynamic problem was also considered previously,[17] but the absorptivity was taken as a constant, thus uncoupling the radiation from the gasdynamics. The present paper extends the analysis of Ref. 17 to variable absorptivity gases for which the radiation and the gasdynamics are closely coupled and presents initial results for some of the simpler cases of interest.

The numerical solution of the completely coupled formulation for absorption in pure hydrogen or argon represents a formidable computational problem that taxes the abilities of the most robust numerical algorithms. The physics of the problem are both complex and diverse and their coupled nature implies that the gasdynamic and radiation equations must be solved simultaneously. Specific difficulties arise from

Presented as Paper 85-1554 at the AIAA 18th Fluid Dynamics and Plasma Dynamics and Lasers Conference, Cincinnati, OH, July 16-18, 1985; received Aug. 5, 1985; revision received April 30, 1986.

*Professor, Department of Mechanical Engineering.
†Graduate Assistant, Department of Mechanical Engineering.

the strong energy source term; the steep temperature gradients and the very high temperature rises; the low Mach number flows that are nonetheless compressible because of the heat addition; the significance of viscosity and thermal conductivity; the radiative losses from the heating region; and the experimental observation that absorption will not occur unless it is initiated by a spark or other breakdown mechanism.

Of these quantities, the energy source term causes difficulties because of its destabilizing influence on the algorithm. The steep temperature gradients require very fine grid resolution in regions whose location is determined by the solution. The low Mach numbers are challenging because of the stiffness they impart to the equations. For example, the powerful compressible flow algorithms that have been developed for transonic flows in the past decade[15,18-20] show poor convergence below Mach numbers of 0.1-0.2. The effects of thermal conductivity are important in determining the propagation rate of the absorption region and require the solution of the complete elliptic equations rather than some simpler version of the equations. The presence of radiation loss does not make the computation more difficult (in fact, this sink term makes it slightly easier), but the accurate representation of radiative transfer in arbitrary directions requires large amounts of CPU time.[21] Finally, our relative unfamiliarity with the character of the solutions and our inability to anticipate when solutions do and and do not exist also adds to the difficulties of computing these interactions. As in the experiments, the computation may be expected to require an appropriate high-temperature "spark" as the initial condition. Further, absorption is not possible for all flow conditions and the failure to converge to a solution may indicate numerical difficulties or simply the absence of a solution, at least for the given initial conditions.

To minimize these problems, the present paper is addressed as absorption in a hydrogen-seedant mixture rather than in a pure gas (Ar or H_2). In particular, the present paper considers the absorption of 10.6 μm radiation in a 99% H_2/1% Cs mixture. This mixture allows much lower peak temperature absorption with correspondingly weaker temperature gradients and energy source terms. Lower heating rates also allow higher flow Mach numbers and much better behaved equation systems. The increased absorptivity at low temperatures implies the absorption region will be primarily propagated by direct absorption from the beam and not by heat feedback. Thus, thermal conduction and elliptic effects are of reduced importance. This also means the absorption process is self-starting and does not require spark initiation. The peak temperatures are also low, thus minimizing radiative losses, but cesium is such a good radiator that there may still be significant radiation losses.

In the following sections, the formulation of the problem and the results of some initial parametric studies are presented.

Problem Formulation

A representative grid system for solving the coupled problem is shown in Fig. 2. Because of the presence of the radiation, two superimposed grids are used. A conventional body-fitted coordinate system is used for the gasdynamics, while the laser beam is split into a series of individual rays. The rays are treated by geometric optics and beam focusing by density gradients in the absorption region is ignored. The equations describing the radiation gasdynamic interaction are given in vector form as

$$\frac{\partial Q}{\partial t}+\frac{\partial E}{\partial \xi}+\frac{\partial F}{\partial \eta}=H+\frac{\partial R}{\partial \xi}+\frac{\partial S}{\partial \eta} \tag{1}$$

for the fluid dynamic variables. The equation for radiation absorption is

$$\frac{1}{c}\frac{\partial IA_\ell}{\partial t}+\frac{\partial IA_\ell}{\partial s}=-kIA_\ell \tag{2}$$

The fluid dynamic equations are written in a body-fitted coordinate system, while the radiation equation applies along individual rays.

In Eq. (1), the vectors Q, E, and F represent the dependent variables in the fluid dynamic equation and their flux vectors in standard form,

$$Q=J^{-1}(\rho,\rho u,\rho v,e)^T \tag{3}$$

and

$$E=J^{-1}\begin{pmatrix}\rho U\\ \rho uU+\xi_x p\\ \rho vU+\xi_y p\\ (e+p)U\end{pmatrix} \qquad F=J^{-1}\begin{pmatrix}\rho V\\ \rho uV+\eta_x p\\ \rho vV+\eta_y p\\ (e+p)V\end{pmatrix} \tag{4}$$

In these expressions, the variables p and ρ represent the pressure and density, respectively, while u and v are the velocity components. The superscript T refers to the transpose of the vector.

The Jacobian of the transformation is denoted by J and is related to the metrics ξ_x, ξ_y, η_x, and η_y as

$$J=\xi_x\eta_y-\eta_x\xi_y \tag{5}$$

The total energy e is defined as

$$e=\rho[\epsilon+(u^2+v^2)/2] \tag{6}$$

where ϵ is the internal energy. The contravariant velocities U and V are given by

$$U=\xi_x u+\xi_y v$$

$$V=\eta_x u+\eta_y v \tag{7}$$

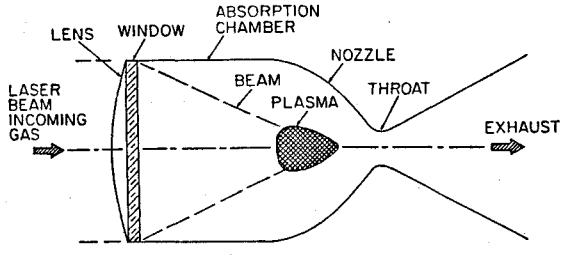

Fig. 1 Radiation gasdynamic interaction in a laser propulsion system.

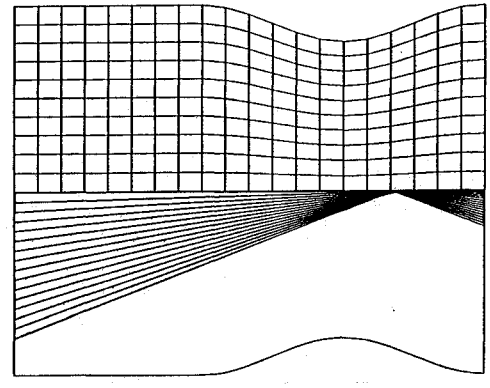

Fig. 2 Nozzle and laser geometry showing fluid dynamic and laser grids (flow is from left to right).

The source term H in Eq. (1) describes the energy deposition from laser absorption. The first three components of this vector correspond to the continuity and the two momentum equations and are zero. Only the fourth component, corresponding to the energy equation, is nonzero. The form of the source term is

$$H = J^{-1}(0,0,0,kI)^T \tag{8}$$

where k is the local absorptivity of the gas at the laser wavelength and I the laser intensity at a particular point in space.

The radiative loss from the hot regions to the walls and to the cooler gas should also appear here, but is ignored in the present analysis as noted above. This allows the emphasis in the present work to be placed on documenting the range of conditions that can be handled computationally.

The viscous terms R and S are given in terms of the Cartesian vectors $\bar{R}$ and $\bar{S}$ as

$$R = J^{-1}(\xi_x \bar{R} + \xi_y \bar{S})$$
$$S = J^{-1}(\eta_x \bar{R} + \eta_y \bar{S}) \tag{9}$$

where

$$\bar{R} = (0,\tau_{xx},\tau_{xy},R_4)^T$$
$$\bar{S} = (0,\tau_{xy},\tau_{yy},S_4)^T \tag{10}$$

The shear stresses are then defined as

$$\tau_{xx} = 4/3\mu u_x - 2/3\mu v_y$$
$$\tau_{xy} = \mu(u_y + v_x)$$
$$\tau_{yy} = -2/3\mu u_x + 4/3\mu v_y \tag{11}$$

and the transport terms in the energy equation are

$$R_4 = u\tau_{xx} + v\tau_{xy} + \kappa T_x$$
$$S_4 = u\tau_{xy} + v\tau_{yy} + \kappa T_y \tag{12}$$

where the second viscosity coefficient λ has been taken as $\lambda = -2/3\mu$ and κ is the thermal conductivity.

The system is closed by specifying an appropriate equation of state and by defining the property variations. For the hydrogen-cesium mixture selected, the effects of the cesium (1%) have been neglected for all properties except the absorptivity. The equation of state is taken as the perfect-gas relation,

$$p = \rho RT/M \tag{13}$$

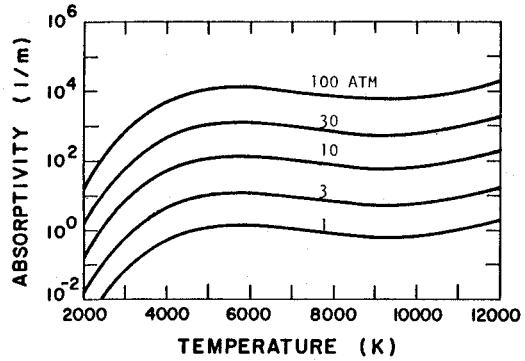

Fig. 3 Absorptivity of equilibrium mixture of 99% H_2/1% Cs (taken from Ref. 5).

with the molecular weight M as well as the internal energy being obtained from thermodynamic relations for equilibrium hydrogen.[5] Conceptually, these functions are given as

$$\epsilon = \epsilon(T,p), \quad M = M(T,p) \tag{14}$$

The viscosity and thermal conductivity are also given as functions of the thermodynamic state,[5]

$$\lambda = \lambda(T,p) \quad \text{and} \quad \mu = \mu(T,p) \tag{15}$$

The equation for radiation conservation at the laser wavelength [Eq. (2)] is valid along any ray of the beam. The dependent variable s represents distance along the ray, while A_ℓ represents the area of the ray. This area is taken to be variable so as to include capability for treating converging beams. The time derivative in Eq. (2) is multiplied by the inverse of the speed of light c. The magnitude of c is large enough that this time derivative can be neglected and the quasisteady form of the radiation equation used. However, this unsteady form is preferred because it facilitates the numerical solution. In the calculations, c is not given its physical value, but rather is selected to accelerate convergence.

For the numerical calculations, it is convenient to divide the radiation equation through by the product IA_ℓ and to convert the dependent variable to the natural logarithm of IA_ℓ rather than IA_ℓ itself. After subdividing the beam into a finite number of rays, we define this new laser power vector as the vector Π, where,

$$\Pi = [\ell n(IA)_1,\ \ell n(IA)_2,\ \ell n(IA)_3,\ldots,\ \ell n(IA)\ldots]^T \tag{16}$$

The number of components in Π corresponds to the number of rays used to simulate the beam. With this notation, Eq. (2) can be rewritten in vector form as

$$\frac{1}{c}\frac{\partial \Pi}{\partial t} + \frac{\partial \Pi}{\partial s} = -K \tag{17}$$

where it is understood that the direction s is different for each ray of the laser. In Eq. (17), the absorptivity has formally been expressed as a vector K to retain consistency.

Applying an Euler implicit scheme in time to Eqs. (1) and (17) and expressing in delta form ($\Delta Q = Q^{n+1} - Q^n$) gives

$$\left[I - \frac{\partial H}{\partial Q}\Delta t + \Delta t\left(\frac{\partial A}{\partial \xi} + \frac{\partial B}{\partial \eta}\right)\right]\Delta Q - \Delta t\frac{\partial H}{\partial \Pi}\Delta\Pi$$
$$= -\Delta t\left[\frac{\partial E}{\partial \xi} + \frac{\partial F}{\partial \eta} - H - \frac{\partial R}{\partial \xi} - \frac{\partial S}{\partial \eta}\right]^n \tag{18}$$

and

$$\Delta t\frac{\partial K}{\partial Q}\Delta Q + \left[\frac{1}{c}I + \Delta t\frac{\partial}{\partial s}\right]\Delta\Pi = \Delta t[K]^n \tag{19}$$

where A and B are standard fluid dynamic Jacobians, $A = \partial E/\partial Q$ and $B = \partial F/\partial Q$, and I is the identity matrix. The superscript n implies evaluation at the nth time level. Although the complete viscous equations are solved, a slip boundary condition is enforced on the walls and the viscous boundary layer is not resolved. Hence, the viscous terms are included only on the right-hand side.

Additional Jacobians that appear are those of the source term with respect to the fluid variables, $\partial H/\partial Q$, as well as with respect to the laser power, $\partial H/\partial\Pi$. The Jacobian of the absorptivity with respect to the fluid variables, $\partial K/\partial Q$, also appears in the laser equation. Note that these latter two Jacobians are not square matrices and, in particular, that the vectors ΔQ and $\Delta\Pi$ are not of equal length. The combined system

[Eqs. (18) and (19)] represents $4+L$ equations (where L is the number of rays into which the laser beam is divided) in the $4+L$ unknowns. Of this number, Eq. (18) represents four equations (continuity, two momentum, and energy) and Eq. (19) represents L equations (one for each ray). These equations cannot be written as a single $4+L$ vector equation because the spatial derivatives in Eq. (19) are each in different directions. Transformation to Cartesian coordinates is possible, but makes it more difficult to ensure energy conservation between the laser and the fluid. To circumvent this, we use separate grids for the laser and the fluid dynamics.

Because of the differences in the grid systems, Eqs. (18) and (19) cannot be coupled at each time step. Instead, we use an iterative procedure at each time level. In the first step, the $\Delta\Pi$ term in Eq. (18) is neglected and the remaining terms are used to obtain a predicted value of ΔQ at each grid point in the field. The presence of the source term $\partial H/\partial Q$ represents the only difference between this step and the traditional methods[15,18-20] for solving the fluid dynamic equations.

Using this value of ΔQ, Eq. (19) is next solved to determine $\Delta\Pi$ and the process repeated using this $\Delta\Pi$ in Eq. (18). The resulting values of $\Delta\Pi$ and ΔQ are taken as the final values at the current time step. In performing these calculations, the differential operators in Eqs. (18) and (19) are replaced by central differences. The very steep nature of the gradients makes the use of central differences almost imperative.

Boundary Conditions

The boundary conditions are enforced by a method of characteristics formulation in the manner described in Ref. 17. Emphasis is placed on choosing boundary conditions that are analogous to realizable experimental conditions. At the upstream boundary, the stagnation pressure and the stagnation enthalpy are specified along with setting the contravariant velocity V to zero. The static pressure is fixed at the downstream boundary. The mass flow is then automatically determined by the back pressure for the particular upstream conditions, the amount of heat addition, and the geometrical configuration. Slip conditions are applied at the nozzle walls as noted earlier. This corresponds to ignoring the effects of the boundary layer. A symmetry condition is used on the centerline so that this boundary is treated as a field point. In all cases where derivatives are required on the boundaries (see Ref. 17), three-point, one-sided derivatives are used to maintain second-order accuracy.

The laser equation requires one upstream boundary condition. In the present calculations, the incoming beam was chosen as Gaussian in shape and the total power in the Gaussian beam was used as a parameter.

Results and Discussion

Solutions have been obtained for the interaction between a flowing gas and a converging beam of laser radiation (10.6 μm) with a Gaussian cross-stream intensity profile. The beam and the working fluid propagate through a nozzle that is composed of a straight inlet followed by a converging-diverging section. The height of the nozzle is given by

$$h/h_0 = 1 \qquad 0 \le x \le x_s$$

$$\frac{h}{h_0} = 1 - \frac{1-A_r}{z}\left[1 - \cos\left(2\pi \frac{x-x_s}{x_f-x_s}\right)\right] \qquad x_s \le x \le x_s \qquad (20)$$

where h_0 is the nozzle height at the inlet, A_r the ratio of the throat area to the inlet area, and x_s and x_f the start and end of the converging-diverging section, respectively. The calculations in this paper were for an inlet height h_0 of 0.10 m, a nozzle length x_f of 0.25 m, and an area ratio A_r of 0.8. The intersection between the straight and curved sections x_s was fixed at 0.10 m. This geometry is shown in Fig. 2. The laser beam width at the inlet (to the $1/e^2$ point of the Gaussian intensity distribution) is 0.16 m. All results presented are for unchoked nozzle flows.

Stagnation conditions are specified at the upstream end and the pressure is specified at the exit. These quantities, along with the laser power, then determine the mass flow in a manner analogous to the experiments. All calculations are for hydrogen gas with 1% cesium, as noted earlier. Real property variations for specific heat, molecular weight, viscosity, and thermal conductivity correspond to those for pure hydrogen.[5] Only the gas absorptivity includes the effects of the cesium. The absorptivity is also taken from Ref. 5 and is shown in Fig. 3. The calculations include molecular transport in the heating zone, but are for slip conditions at the nozzle walls.

Detailed Flowfield Characteristics for One Condition

The detailed flowfield characteristics for a representative case are shown in Fig. 4. The flow is from left to right and only the bottom half of the symmetric nozzle is shown. The calculations in this figure are for a nozzle pressure ratio (p°/p) of 1.2, an inlet stagnation temperature of 2200 K, and a pressure of 25 atm. The laser power is 600 MW/m. Figure 4a shows the temperature contours, Fig. 4b the contours of the heat added per unit volume, Fig. 4c the laser intensity contours, Fig. 4d the Mach number contours, and Fig. 4e the streamline shapes. The beam edge and the focal point are shown in each plot.

The temperature profiles show the expected shape with strong heating on and near the nozzle centerline. The omission of radiation loss results in temperature contours that do not close downstream (as contrasted with the experimental contours of Keefer et al.[6]), but the peak temperatures are much lower, nominally around 3700 K. The steepest temperature gradients are seen to be in the radial direction and arise because of beam edge effects.

The heat absorption per unit volume for this case is shown in Fig. 4b. As can be seen, the rate of heat addition increases to a maximum about halfway to the focal point and then decreases to almost zero by the time it reaches the focal point. This confinement of absorption to the portion of the beam in front of the focus is not a general result that occurs in all cases, as is noted later. Instead, its distribution is determined by the product of the local absorptivity and the local laser intensity. As the gas moves the nozzle, its absorptivity increases because of the heating. At the same time, the laser intensity may either increase or decrease, depending upon whether or not the power lost from the beam compensates for the geometric convergence. In this particular case, the laser power is nearly totally absorbed upstream of the focal point and the heat absorption drops to zero.

The manner in which the laser intensity varies for this case is shown on Fig. 4c. The intensity initially increases because the geometric convergence of the beam is stronger than the absorption, but eventually reaches a peak and rapidly drops to zero. This same information is replotted in different form in Fig. 5. Here, the cross-beam intensity distribution is given at several x locations. The intensity of the nonabsorbed beam is also given for reference. The initial Gaussian profile is shown at the upstream end ($x=0$). The next profile is at $x/L=0.23$. At this location, the intensity on the axis of symmetry is higher than at the inlet plane and the beam is narrower because of beam convergence. A small fraction of the beam has already been absorbed, as can be seen by comparing the solid curve with the dashed one.

The third x location shown is at $x/L=0.39$. For this case, the nonabsorbed beam has been omitted for clarity, but the qualitative effects of absorption are clearly shown. The peak intensity no longer occurs on the centerline and the intensity is everywhere lower than it was at the inlet. The fourth curve, at $x/L=0.5$, is much lower than its nonabsorbed counterpart, with the peak intensity still farther from the axis. The final curve, for $x/L=0.76$, shows that nearly the entire beam has been absorbed. The reason the central portion of the beam is

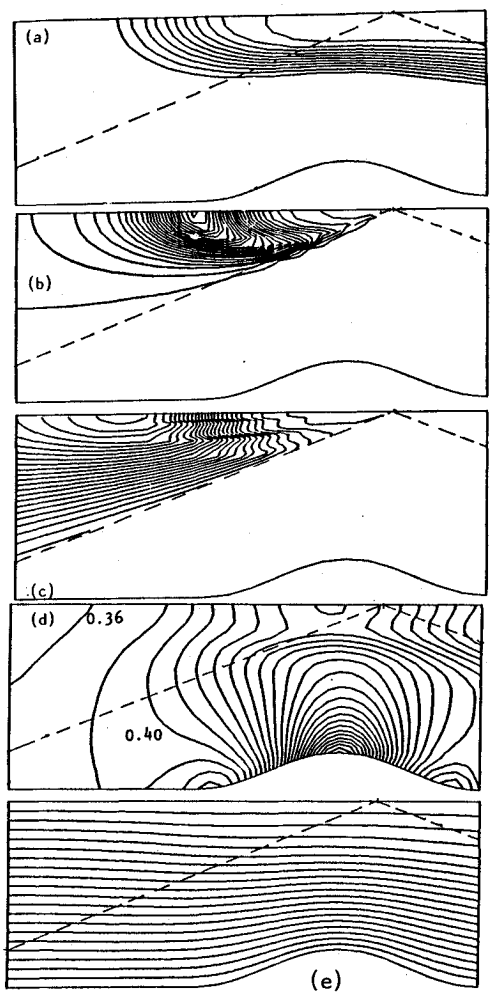

Fig. 4 Detailed flowfield characteristics for representative calculation (inlet temperature, 2200K; pressure, 25 atm; nozzle pressure ratio, 1.2; laser power, 600 MW/m; dashed line indicates beam edge): a) temperature; b) heat absorbed per unit volume; c) laser intensity; d) Mach number, $\Delta M = 0.02$; e) streamlines.

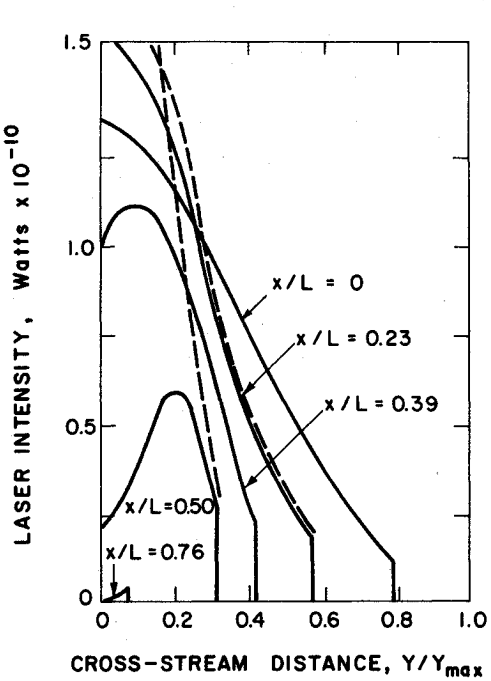

Fig. 5 Cross-stream intensity distribution at various axial locations for case shown in Fig. 4 (dashed line represents intensity of unabsorbed beam).

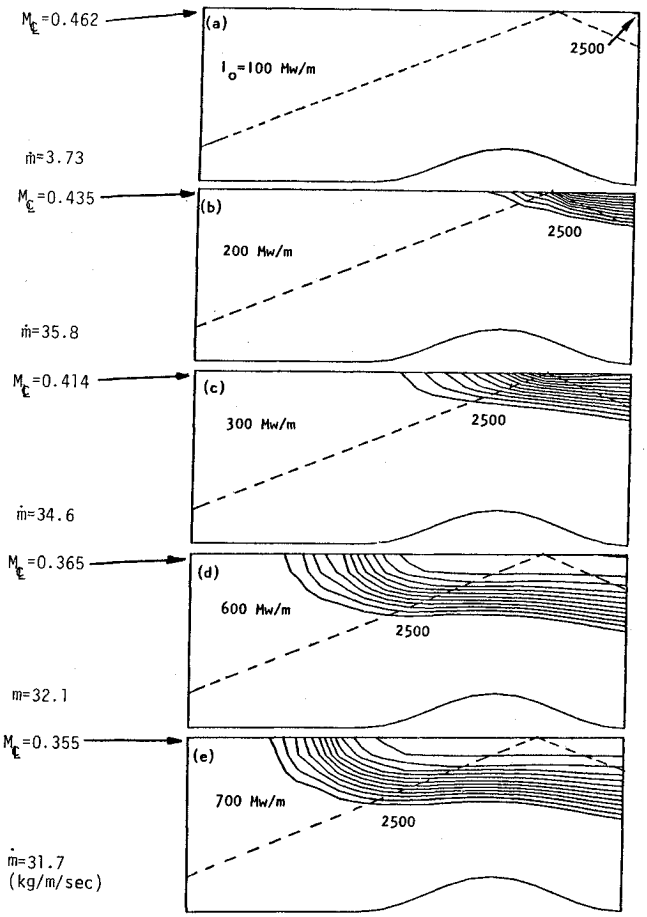

Fig. 6 Parametric study of laser power variations ($T_{IN} = 2200$ K, $p = 25$ atm, $p^\circ/p = 1.2$; dashed line indicates beam edge; temperature increment is 100 K).

absorbed more rapidly than the outer parts (as shown in the last three curves) is because the temperature is a maximum on the centerline. For reference, the focal point occurs at $x/L = 0.40$.

Returning to Fig. 4, the corresponding Mach number contours for this case are shown in Fig. 4d. The level of the Mach number is above 0.4, but there is no difficulty in maintaining the absorption region at these relatively high velocities in this hydrogen-seedant mixture. The variation in Mach number that is observed is primarily because of the nozzle convergence; the laser heat addition has little effect. The heat addition does, however, cause the Mach number on the centerline to increase somewhat above its no-heat case (at constant nozzle pressure ratio), even though the total mass flow decreases with heating.

The streamline plot in Fig. 4e shows that this degree of heating has little impact on the streamline paths, although there is a tendency for the gas to move away from the nozzle centerline and "go around" the heating zone.

A final comment concerning the present example is that the pressure field (not shown) is almost unaffected by the heating. The only notable pressure variation in the flowfield is that caused by the nozzle area change. This observation is in agreement with the familiar approximation in combustion applications that low Mach number heat addition is a constant pressure process. This qualitative statement concerning pressure also holds true for the other cases presented here.

Movement of Absorption Region with Variations in Laser Power

A series of calculations at a pressure of 25 atm, an inlet stagnation temperature of 2200 K, and a nozzle pressure ratio

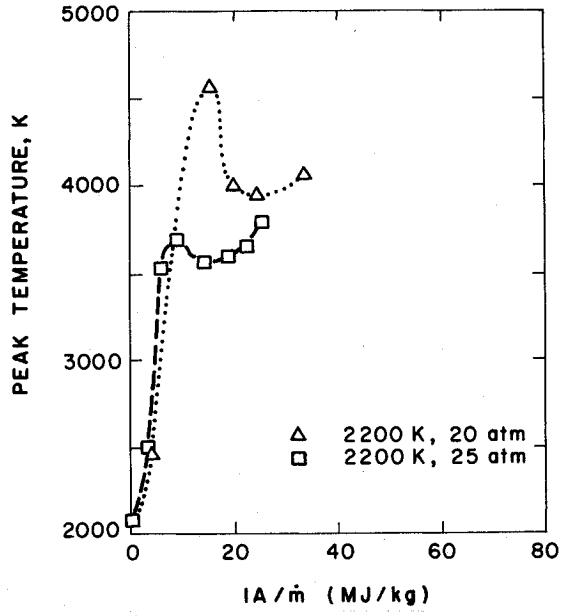

Fig. 7 Peak temperature vs laser power to mass flow ratio for 20 and 25 atm ($T_{IN} = 2200$ K, $p^\circ/p = 1.2$).

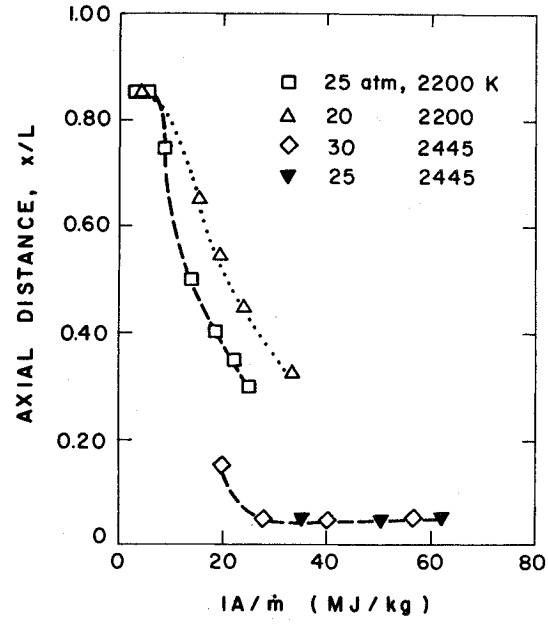

Fig. 8 Movement of peak absorption location as a function of laser power to mass flow ratio ($T_{IN} = 2200$ K, $p^\circ/p = 1.2$).

of 1.2 have been made to show the manner in which the absorption region moves as the laser power is varied. Temperature contour plots for five of these cases are shown in Fig. 6. Starting from the contour plot at the top (Fig. 6a) and moving to the one at the bottom, the laser power is continuously increased from 100 to 700 MW/m. At the lowest laser power (100 MW/m), the laser passes through the flowfield with almost no absorption. Only a very tiny region of heating appears at the downstream end of the flowfield. Although the grid is not sufficiently refined to resolve heating regions this small, the results should be qualitatively correct. This absorption region is seen to reside entirely downstream of the focal point, in contrast to classical arguments[9,10] that it would be unstable here. Of course, if lower temperature contours were plotted, they would show some heating in front of the focal point as well; but for consistency in comparing the various cases, similar temperature contours are shown in all figures.

The temperature contours in Fig. 6b are for a laser power that is twice that of Fig. 6a, namely 200 MW/m. Here, the lowest temperature contour (2500 K) lies in front of the focal point, although a substantial fraction of the heating still occurs in the downstream section. The peak temperature is higher than in Fig. 6a, as is the fraction of power absorbed.

Moving on to Fig. 6c where the laser power is 300 MW/m, we see a further upstream advance in the heating region location. The temperature increase on the centerline continues to be quite rapid until near the focal point, indicating that substantial power remains in the beam up to this point.

Additional increases in laser power continue to move the heating zone forward as shown in Figs. 6d and 6e. The nearly constant temperature region on the centerline at the downstream end of the nozzle indicates that the power in the beam is almost totally absorbed. Figure 6d, which is for a power of 600 MW/m, is the case shown in Fig. 4. Figure 6e is for 700 MW/m.

Attempts at calculating powers above 700 MW/m failed to converge, but the manner in which they behaved is interesting. At higher laser powers, the heating zone appears to jump from a temperature profile like that shown in Fig. 6e to one where the heating occurred very near the upstream boundary. However, rather than staying at this forward location, it appeared to oscillate between these two locations and, hence, prevented convergence. Although these calculations are time dependent, they are far from being time accurate during a transient (in fact, considerable effort has been spent in making the transient inaccurate in exchange for faster convergence) and we cannot interpret this convergence failure as a physical instability. Nevertheless, computations of other flowfields (such as the wake behind a cylinder) have shown a similar refusal to converge when the Reynolds number is raised to levels at which an unsteady vortex street appeared and steady solutions no longer exist. Thus, the present convergence failure could be a suggestion that stable solutions no longer exist or it could be an indication of difficulties with the numerical algorithm. Time-accurate transient calculations are needed to resolve this issue.

Effects of Pressure and Laser Power on Peak Temperature and Absorption Location

Figures 7 and 8 show the manner in which the peak temperature in the flowfield and the location of peak heat addition vary with laser power for two different pressures, 20 and 25 atm. The 25 atm data correspond to the results shown in Fig. 6. The 20 atm data represent an analogous sequence of calculations at a lower pressure. The peak temperature and the location of peak heat addition are obvious scalar parameters of interest, but the latter deserves some additional comment. In principle, the location of peak heat addition could occur anywhere in the nozzle; but for focused Gaussian beams it is constrained to occur on the axis of symmetry. Therefore, in Fig. 8 only the x location of the position of peak heat addition is indicated. Note also that the location of peak heating corresponds to the position of the maximum on contour plots like that in Fig. 4b (heat deposition per unit volume).

Starting from zero laser power where the entire temperature field remains at the inlet temperature, the peak temperature increases rapidly with laser power at first and then becomes more or less constant (see Fig. 7). The region of rapid increase corresponds to conditions like those shown in Figs. 6a and 6b. At these low laser powers, there are several factors that combine to cause the peak temperature to rise with increasing laser power. The first is the obvious factor that the peak temperature rises because there is more power available. Second, the absorption zone is just becoming established at these laser powers and the fraction of power absorbed is increasing from 0 to 100%. Thus, the total power deposited in the gas is increasing at a rate much larger than the increase in power in

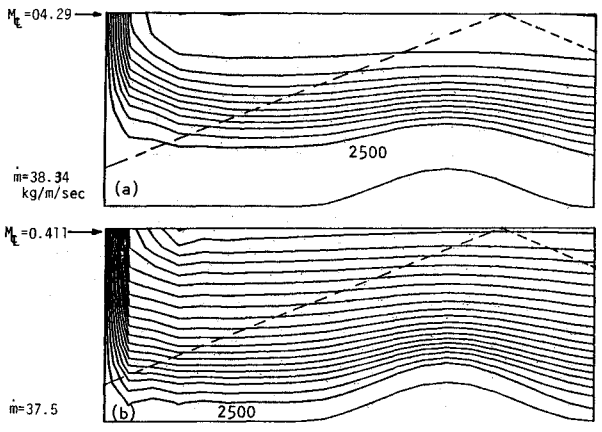

Fig. 9 Temperature contours for 30 atm case ($T_{IN}=2445$ K, $p°/p=1.2$, $\Delta T=100$ K) at laser powers of a) 100 MW/m and b) 200 MW/m.

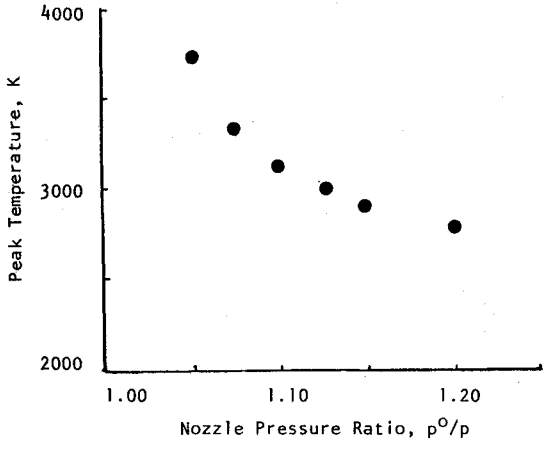

Fig. 10 Effect of nozzle pressure ratio on peak temperature ($T_{IN}=2445$ K, $I_0=100$ MW/m, $p=12$ atm).

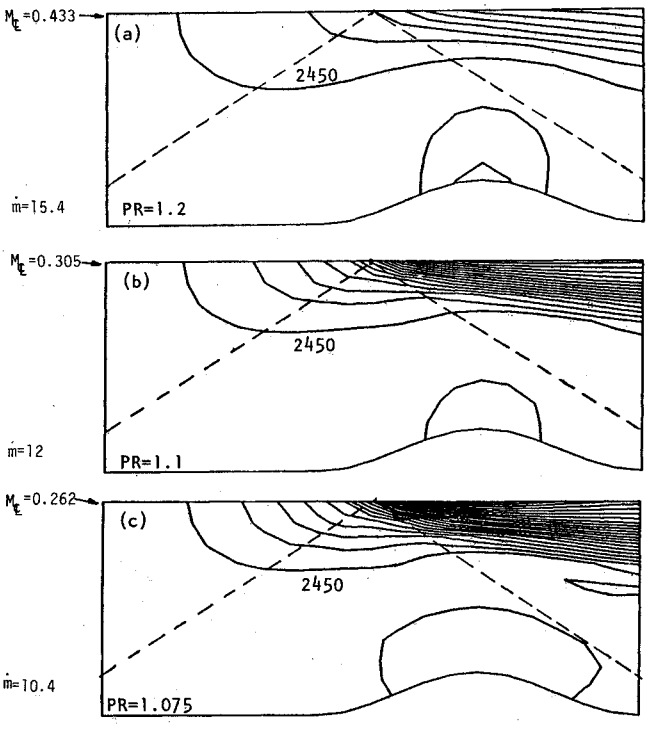

Fig. 11 Temperature contours for various nozzle pressure ratios ($T_{IN}=2445$ K, $I_0=100$ MW/m, $p=12$ atm, $\Delta T=50$ K).

the incoming beam. Third, as the absorption region moves forward from the rear of the nozzle toward the focal point, the local area of the beam gets smaller and the energy is deposited in a smaller volume of gas. This movement of the absorption zone is indicated in Fig. 8.

The region in which the peak temperature is nearly constant is one in which the heating zone is moving rapidly forward, as can be seen from Fig. 8. For these laser powers, the fraction of power absorbed remains at 100%, but the increases in incoming power are offset by the increasing volume of fluid that is heated as the absorption region moves from the focal point where the beam is narrow to the upstream boundary where it is much more diffuse.

For the purpose of making comparisons at the two different pressure levels, the laser power in Figs. 7 and 8 has been normalized by the mass flow $IA/\dot{m}$. (For a fixed nozzle pressure ratio, the mass flow decreases in proportion to the pressure if heat addition is neglected.) Thus, if the laser power were uniformly distributed over all the mass in the nozzle, equal values of $IA/\dot{m}$ would correspond to equal temperature rises. Figure 7 shows that even when normalized in this manner, the peak temperatures are higher at the lower pressures. However, the thermodynamic energy balance is not the only factor that determines the heating characteristics. In addition to decreasing the mass flow, the reduction in pressure also decreases the absorptivity, as seen from Fig. 3. Figure 8 shows that this lower absorptivity causes the location of peak heat addition to lie further aft at the lower pressure. Thus, the absorption zone for the lower-pressure case is situated in a region where the laser beam is narrower and the resulting temperature rise is larger.

Also shown in Fig. 8 are data for an inlet temperature of 2445 K at pressures of 25 and 30 atm. Comparison of the two sets of data for 25 atm shows that increasing the inlet temperature causes the absorption zone to move forward. Once again, this forward movement occurs because an increase in the inlet temperature corresponds to increasing the absorptivity (see Fig. 3); this agrees with the results found for the effect of pressure. At the higher inlet temperature, the peak absorption location lies very close to the upstream boundary. The change from 25 to 30 atm should accentuate this shift, but the results show that a further increase in absorptivity (by increasing pressure) does not affect the peak absorption location. This suggests that the absorption zone location is being dictated by the upstream boundary. To give an indication of the shape of the temperature contours in this upstream limit, temperature contours for the largest and smallest laser power cases at 30 atm are shown in Fig. 9.

Effect of Gas Velocity

The results of a parametric study of the effect of gas velocity on the absorption process are shown in Figs. 10 and 11. These results are for a fixed-laser intensity of 100 MW/m and an inlet temperature of 2445 K. The pressure for these calculations was 12 atm and the focal point was situated at the midpoint of the nozzle substantially upstream of its location in the previous results. The velocity changes were imposed by varying the nozzle back pressure, while holding the upstream stagnation pressure fixed. The results are plotted as a function of the nozzle pressure ratio, $p°/p_B$. The variation of peak temperature with nozzle pressure ratio is shown in Fig. 10. As the velocity is reduced (i.e., as the nozzle pressure ratio is decreased from 1.2 to 1.05), the peak temperature increases substantially. These higher temperatures occur because the increased gas transit time through the nozzle allows each fluid element to absorb more photons. Also note that reducing the nozzle pressure ratio while holding the laser power fixed cor-

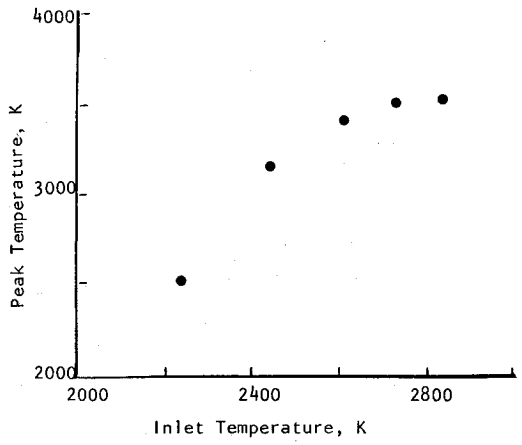

Fig. 12 Variation of peak temperature with inlet temperature ($I_0 = 100$ MW/m, $p = 12$ atm, $p^\circ/p = 1.1$).

responds to increasing the ratio $IA/\dot{m}$, again suggesting increased temperatures.

Temperature contours for three of the cases shown in Fig. 10 are given in Fig. 11. The revised location of the focal point is noted on these curves. Note that a different spacing ($\Delta T = 50$ K) has been used. For all three flow velocities shown, the majority of the heating occurs downstream of the focal point. Again, the convergence rate for these cases suggests that these zones are stable to disturbances.

Effect of Variations in the Inlet Temperature

The effect of variations in the inlet temperature on the peak temperature is shown on Fig. 12. Variations in the inlet temperature at about 2200-2850 K cause the peak temperature to increase rapidly at the lower temperatures and more slowly at the higher temperatures. The major physical effect of the increased inlet temperature is to increase the absorptivity of the gas. As noted earlier, increased absorptivity tends to move the absorption region forward. The calculations in Fig. 12 are for a pressure of 12 atm, an incoming laser power of 100 MW/m, and a pressure ratio of 1.1. These calculations were performed with the beam focus at the point indicated in Fig. 11.

Summary and Conclusions

The interaction between a focused laser beam and a flowing gas has been analyzed by means of a two-dimensional numerical model. Hydrogen gas seeded with 1% cesium has been used as the working fluid. The cesium provides significant absorption in the low-temperature ranges and allows stable heating at relatively high subsonic Mach numbers. The peak temperatures reached with this mixture are quite low, typically in the range of 3500-4000 K for the cases calculated. Both the high velocity and the low peak temperature make the numerical solution easier. Real-gas properties corresponding to those of equilibrium hydrogen were used for all quantities except the absorptivity, for which properties of the hydrogen/cesium mixture were used.

By varying various parameters, it was possible to position the absorption region any place in the flowfield from the downstream end to the upstream end. In general, any change that causes the absorptivity to increase will also tend to move the absorption region forward. Examples of such changes include increasing the gas pressure, inlet temperature, or laser power. The peak temperature may also increase with these parameters, but forward movement of the absorption zone in the converging part of the beam causes the energy to be deposited in a larger volume of gas, thus counteracting the temperature rise. The cases computed included ones for which the absorption occurred primarily in the diverging section of the beam downstream of the focal point and these solutions appeared to be stable.

The pressure calculations were all for laser beams with Gaussian intensity distributions at the inlet plane. Focused beams with maximum intensity in the center ensure that the peak temperature in the flowfield will occur on the symmetry plane, but these higher temperatures also lead to preferential absorption on the symmetry plane. As the beam propagates through the gas, the power in the center is absorbed more rapidly, so that the partially attenuated beam may take on a "donut"-shaped profile with maximum power in some off-axis position and a point of relative minimum at the center.

Extension of the present analysis to conditions analogous to those being used in current experiments in hydrogen and argon[6-8] is being attempted, but it appears that the numerical algorithm will have to be modified considerably to obtain solutions at these very low-velocity conditions. Modifications allowing rapid convergence at Mach numbers as low as 10^{-4} have been developed and are currently being tested.

Acknowledgment

This work was sponsored by the U.S. Air Force Office of Scientific Research under Grant AFOSR 82-0196 and by NASA through CFD Training Grant NGT 39-009-802.

References

[1]Jones, L. W. and Keefer, D. R., "NASA's Laser-Propulsion Project," *Astronautics and Aeronautics*, Vol. 20, Sept. 1982, p. 66.

[2]Kemp, N. H., Rosen, D. I., and Legner, H. H., "Laser Energy Absorption in Gases: Research Problems," *AIAA Progress in Astronautics and Aeronautics: Orbit Raising and Maneuvering Propulsion: Research Status and Needs*, edited by L. H. Caveny, Vol. 89, AIAA, New York, 1984, pp. 73-94.

[3]Keefer, D., Elkins, R., Peters, C., and Jones, L., "Laser Thermal Propulsion," *AIAA Progress in Astronautics and Aeronautics: Orbit Raising and Maneuvering Propulsion: Research Status and Needs*, edited by L. H. Caveny, Vol. 89, AIAA, New York, 1984, pp. 129-148.

[4]Merkle, C. L., "The Potential for Using Laser Radiation to Supply Energy for Propulsion," *AIAA Progress in Astronautics and Aeronautics: Orbit Raising and Maneuvering Propulsion: Research Status and Needs*, Vol. 89, edited by L. H. Caveny, AIAA, New York, 1984, pp. 48-72.

[5]Kemp, N. H. and Krech, R. H., "Laser Heated Thruster—Interim Report," NASA CR-161666, Sept. 1980.

[6]Keefer, D., Crowder, H., and Peters, C., "Laser Sustained Argon Plasmas in a Forced Convection Flow," AIAA Paper 85-0388, Jan. 1985.

[7]Krier, H., Mazumder, J., Glumb, R. J., Bender, T. D., and Rockstroh, T. J., "Experiments in Plasma Initiation and Laser Absorption in Flowing Gases," University of Illinois, Urbana, Annual Tech. Rept. UILU-ENG-85-4004, April 1985.

[8]VanZandt, D. M., McCay, T. D., and Eskridge, R. H., "An Experimental Study of Laser-Supported Hydrogen Plasmas," AIAA Paper 84-1572, June 1984.

[9]Kemp, N. H. and Root, R. G., "Analytical Study of Laser-Supported Combustion Wave in Hydrogen," *Journal of Energy*, Vol. 3, Jan.-Feb. 1979, pp. 40-49.

[10]Raizer, Yu. P., *Laser-Induced Discharge Phenomena*, edited by G. C. Viases, and Z. A. Pietrzyk, Consultants Bureau, New York, 1977, pp. 26-44.

[11]Jackson, J. P. and Nielsen, P. E., "Role of Radiative Transport in the Propagation of Laser-Supported Combustion Waves," *AIAA Journal*, Vol. 12, Nov. 1974, pp. 1498-1501.

[12]Gulati, A. and Merkle, C. L., "The Absorption of Electromagnetic Radiation in an Advanced Propulsion System," *Journal of Spacecraft and Rockets*, Vol. 21, Jan.-Feb. 1984, pp. 101-107.

[13]Merkle, C. L., "Prediction of the Flowfield in Laser Propulsion Devices," *AIAA Journal*, Vol. 22, Aug. 1984, pp. 1101-1107.

[14]Merkle, C. L., Gulati, A., and Choi, Y.-H., "The Effect of Strong Heat Addition on the Convergence of Implicit Schemes," *AIAA Journal*, Vol. 23, June 1985, pp. 847-855.

[15]Beam, R. M. and Warming, R. F., "An Implicit Factored Scheme for the Compressible Navier-Stokes Equations," *AIAA Journal*, Vol. 16, April 1978, pp. 393-402.

[16]Batteh, J. H. and Keefer, D. R., "Two-Dimensional Generalization of Raizer's Analysis for the Subsonic Propagation of Laser Sparks," *IEEE Transactions on Plasma Science*, Vol. PS-2, Sept. 1974.

[17]Merkle, C. L., Molvik, G. A., and Choi, D., "A Two-Dimensional Analysis of Laser Heat Addition in a Constant Absorptivity Gas," *AIAA Journal*, Vol. 23, July 1985, pp. 1053-1060.

[18]Briley, W. R. and McDonald, H., "On the Structure and Use of Linearized Block Implicit Schemes," *Journal of Computational Physics*, Vol. 34, 1980, pp. 54-73.

[19]Steger, J. L., "Implicit Finite-Difference Simulation of Flow about Arbitrary Two-Dimensional Geometries," *AIAA Journal*, Vol. 16, July 1978, pp. 679-686.

[20]Pulliam, T. H., Jespersen, D. C., and Childs, R. E., "An Enhanced Version of an Implicit Code for the Euler Equations," AIAA Paper 83-0344, Jan. 1983.

[21]Merkle, C. L. and Choi, Y.-H., "Computation of Compressible Flows at Very Low Mach Numbers," AIAA Paper 86-0351, Jan. 1986.